



Advanced Microtexture Evaluation of Dextran Biofilms Obtained from Low Cost Substrate Loaded with *Maytenus rigida* Extract

Mário R. P. Silva^a, Robert S. Matos^{a,b} , Erveton P. Pinto^b, Samuel B. Santos^c,
Michael D. S. Monteiro^d, Henrique D. da Fonseca Filho^{e*} , Luiz E. Almeida^a

^aUniversidade Federal de Sergipe (UFS), Programa de Pós-graduação em Ciência dos Materiais e Engenharia, São Cristóvão, SE, Brasil.

^bUniversidade Federal do Amapá (UNIFAP), Grupo de Materiais Amazônicos, Departamento de Física, Macapá, AP, Brasil.

^cUniversidade Federal de Sergipe (UFS), Programa de Pós-Graduação em Ciências dos Materiais e Engenharia, São Cristóvão, SE, Brasil.

^dUniversidade Federal de Sergipe (UFS), Programa de Pós-Graduação em Química, São Cristóvão, SE, Brasil.

^eUniversidade Federal do Amazonas (UFAM), Laboratório de Síntese de Nanomateriais e Nanoscopia, Departamento de Física, Manaus, AM, Brasil.

Received: December 29, 2020; Revised: February 25, 2021; Accepted: April 27, 2021

We have obtained kefir biofilms loaded with *Maytenus rigida* extract. The main goal was to evaluate the influence of the addition of the extract on the biofilms microtexture using stereometric and fractal parameters. Atomic force microscopy, Fourier transform infrared spectroscopy, and contact angle techniques were used to evaluate the topography, chemical interaction and wettability of the biofilms. Chemical evaluation showed that the extract interacts with the polymeric matrix of the biofilms, changing their structure. This behavior affected the surface energy because the wettability decreased when the *Maytenus* content increased. The surface morphology was also affected and suggested the prevalence of bacteria and yeast at lower and higher extract concentrations, respectively. The surface roughness increased according to the increase in the extract concentration. Texture parameters revealed that the biofilm with lowest concentration had deeper furrows than for higher concentration. Advanced fractal parameters revealed that topographic uniformity, percolation and texture homogeneity were more suitable for the biofilm with 0.25 g.L⁻¹ of extract. These results indicate that this biofilm has promising 3D micromorphology for regenerative medicine application. Furthermore, the physics tools used revealed to be very useful for characterizing of the microtexture of polymeric-based biological materials.

Keywords: *Kefir Biofilms, Maytenus rigida, Atomic force microscopy, Stereometric, Fractal parameters.*

1. Introduction

Kefir is a fermented drink produced from kefir grains and they are constituted by colonies of lactic bacteria. These microorganisms produce a polysaccharide matrix that changes according to the substrate on which kefir grains are grown (e.g., “Kefiran” of dairy substrate grains¹ and “Dextran” of water kefir grains²) and has been recently studied a lot. This polysaccharide has been used in the development of biofilms for application in the food industry and more recently as potential natural skin dressing^{3,4}. Its structure can be composed for equal amounts of glucose and galactose with rings that are interleaved in the structure of the biopolymer. Piermaria et al.¹ showed

that kefir films have pseudoplastic behavior, with good characteristics for use in plastic films. In addition, the film produced with glycerol exhibited excellent plastic quality, compared to that of another polymer such as polyethylene. Likewise, Ghasemlou et al.⁵ also observed this feature in kefir. This behavior was attributed by Pop et al.⁶ for the functional groups that form the exopolysaccharide matrix of this biopolymer. Similarly, Coma et al.² showed that Dextran has great elastic properties to be used as food packaging in the food industry.

Several previous works demonstrate that Dextran has a proven activity as a natural regenerative agent, however, in general the routes for obtaining the material are not very

*e-mail: hdfilho@ufam.edu.br

ecofriendly. In the last decade, dextran-based scaffolds for tissue repair has become a viable alternative⁷, but the preparation of hydrogels and films for cell anchoring has been much more explored. Draye et al.⁸ showed that Dextran dialdehyde cross-linked gelatin hydrogel was designed to have good biocompatibility, since after 16 days of implantation of the biomaterial a satisfactory regenerative response was observed. Brunsen et al.⁹ developed photocrosslinkable dextran hydrogel films as an effective surface for cell anchoring, where the authors showed that crosslinking by irradiation with ultraviolet light promoted the formation of substrates with excellent biological responses. Zheng et al.¹⁰ produced a composite based on Dextran-aldehyde to be used as an effective wound dressing, where the result was a material with a highly porous structure, strong resistance to traction, low toxicity, and good biocompatibility. Furthermore, in vivo essays showed that after 10 days an almost complete wound healing was achieved in the study. More recently, Tchobanian et al.¹¹ fabricated Dextran-based films standardized using thermal nanoimprint lithography (T-NIL) and revealed that the films had character moderately hydrophobic, with low surface roughness and proved that the polysaccharide matrix can support cell adhesion and anchorage.

Naturally, research has evolved and more ecofriendly routes for obtaining this biopolymer have been considered. Matos et al.⁴ produced kefir biofilms associated with *Theobroma grandiflorum* Shum and *Euterpe oleracea* Mart. extracts using brow sugar as substrate and show that they may have applications in the biomedical field. Almeida et al.¹² concluded that the best concentration of kefir grains for production and biofilms with brow sugar was 40 g.L⁻¹. Ferraro et al.¹³ demonstrated that bacteria are distributed along the surface of biofilms fabricated with brow sugar in low concentrations of grains in the film-forming solution, more specifically between 10 g.L⁻¹ and 40 g.L⁻¹. These results have revealed that this probiotic has great potential for biomedical application. However, of the three most common types of sugar used to fabricate kefir biofilms such as brown, demerara and white (refined) sugar, brown sugar is the most expensive, which can make the process of fabrication these biofilms more unfeasible. Demerara sugar, in addition to undergoing a minor refining process, is a sugar with a lower cost and almost equivalent in price to commercial refined sugar, which makes it a more viable alternative for the fabrication of biofilms of biomedical interest.

On the other hand, *Mautenus rigida* Mart., which is popularly known as “chápeu de couro”, is a plant well known in the population of northeastern Brazil¹⁴, and it provides an extract rich in Tannins and triterpenes¹⁵. These compounds have been attributed to strong antimicrobial activity against some pathogens such as *Staphylococcus aureus*, *Escherichia coli*, *Pseudomonas aeruginosa*, and strains of *Salmonella sp*^{16,17}.

Film surface studies have revealed that some parameters such as height, feature, spatial, volume, hybrid, and functional may vary according to the synthesis method^{18–20}. Atomic force microscopy technique has been an ally in the investigation of biological systems because it is a very sensitive and nanometer scale technique that allows to characterize biofilms at cellular level with high resolution²¹. The morphology surface study

is essential to understand certain aspects of the surface of these systems, e.g., surface roughness, surface asymmetry, microtexture, particles.

Biofilms are complex systems whose formation process is microscopically much discussed today. Furthermore, the morphology of biological based-systems on image processing has been extensively studied with the use of AFM, e.g.,^{22–25}. Fractal geometry, in turn, has been widely used to complement morphological analysis on the microtexture of others systems, e.g.,^{26–31}. The fractal theory has provided a more direct understanding of the surface microtexture and its relationship with the method of synthesis and formation of films at micro and nanoscale, through fractal dimension analysis^{29,32}.

For all these reasons, we prepare kefir microbial biofilms grow on demerara sugar solution loaded with hydroethanolic extract of *Maytenus rigida* Mart.. Our main goal was to evaluate the influence of the plant extract incorporation on the microtexture of this biological system, using stereometric and fractal parameters. Before this, we explore the effects of Maytenus's content on the structure and wetability of the films. All statistical stereometric parameters were evaluated according to the international standard ISO 25178-2: 2012. Furthermore, three new fractal parameters, which are not provided by commercial software, have been introduced, such as surface entropy, fractal succolarity, and fractal lacunarity.

2. Materials and Methods

2.1. Material

The water kefir grains were obtained in a holdhouse. They were kept in demerara sugar solution for 15 days to maintain the viability of the grains. *Maytenus rigida* Mart. Was extracted from 2kg of barks obtained in the OLHO D'AGUA CASADO settlement, located at 09 ° 38'31 " S and 37 ° 47'18 " W, Canindé do São Francisco, State of Sergipe-Brazil. The specie was identified at the Federal University of Sergipe-UFS Herbarium (ID 00767). The bark was kiln dried at 37°C and then was reduced to powder ~ 530g using a knife mill. The extract was obtained by alcohol precipitation in ethanol solution (90%) for 6 days at room temperature in a closed bottle. Finally the extract was filtered and centrifugated in a rotatory evaporator under reduced pressure at 50 °C. The resulting extract was stored in all falcom until its use in formulations of filmogenic solutions. The phytochemical characterization of this extract was previously discussed by Santos³³.

2.2. Biofilm preparation

There is several routes to synthesize polysaccharides-like Dextran. In this work, we have obtained Dextran using a ecofriendly route because Dextran biofilms were obtained from water kefir grain. The biofilms synthesis was carried out according to methods previously employed, e.g.,^{34–36}. The substrates were prepared keeping the demerara sugar concentration constant at 40 g.L⁻¹. The first biofilm was prepared by mixing 40 g.L⁻¹ of water kefir grains in a solution of demerara sugar and distilled water and it was named Bio0. Subsequently, the other 3 solutions were prepared with

different concentrations of *Maytenus rigida* Mart. extract, such as 0.25 g.L⁻¹, 0.50 g.L⁻¹, and 0.75 g.L⁻¹. The grains were also inoculated and then the film-forming solutions were sealed in 3000 mL bottles and kept at temperature of 27 ± 2 °C for 25 days. After this period, the biofilms were carefully removed and dried in an oven at 37 ± 2 °C for 48 hours. These biofilms were named Bio25, Bio50, and Bio75. The aspect of the developed films can be seen in Figure 1.

2.3. FTIR analysis

Maytenus rigida Mart. powder spectrum was obtained using a Shimadzu, Modelo: IRPrestige-21 operating in a range of 400-4000 cm⁻¹, using a resolution of 16 cm⁻¹, and scan rate of 64 s⁻¹. EPS-Based films spectra were recorded using a Shimadzu FTIR Spectrometer model IRAffinity-1, over the range 650-4000 cm⁻¹, with a resolution of 4 cm⁻¹, and scan rate of 64 s⁻¹. In all cases, four measures were taken for comparison of data representativeness.

2.4. AFM analysis

The topographic mapping was performed in an AFM Bruker Dimension Edge in tapping mode operation with a standard silicon cantilever RFESPA (Bruker, spring constant ~3 N/m, tip radius ~8 nm, frequency ~ 75 kHz). The linear scanning rate was set to 0.5 Hz (1 line/s) with a pixel number of 512 × 512 and the mapping of the material was performed at 30x30 μm² scan size. The samples were cut into rectangular pieces of 2 x 2 cm² squares and deposited using double-sided tape on glass plates. Four different measurements were made in random regions of the biofilms to assess the representativeness of the most relevant measure of the surface morphology. Then, images were analyzed with MountainsMap Premium software version 8.4.8872, according to ISO 25178-2: 2012³⁷⁻³⁹.

2.4.1. Roughness Parameters

The surface mapping was carried out by determining the surface roughness parameter and asymmetry as such as root mean square roughness (S_q) and surface skewness (R_{sk}) that were computed by Equations 1 and 2.

$$S_q = \sqrt{\frac{1}{a} \iint_a Z(x,y) dx dy} \quad (1)$$

$$R_{sk} = \frac{\frac{1}{a} \iint_a Z^3(x,y) dx dy}{S_q^3} \quad (2)$$

where $Z(x,y)$ is the height function of the vertical profile and a is the scan area⁴⁰. The average value of each parameter was obtained from five measurements of each biofilm. All these parameters were determined by the MountainsMap Premium software trial version 8.4.8872.

2.5. Topographic homogeneity

The height distribution is a parameter that can affect the homogeneity of the surface energy. Surfaces with topographic heterogeneity cause problems with surface

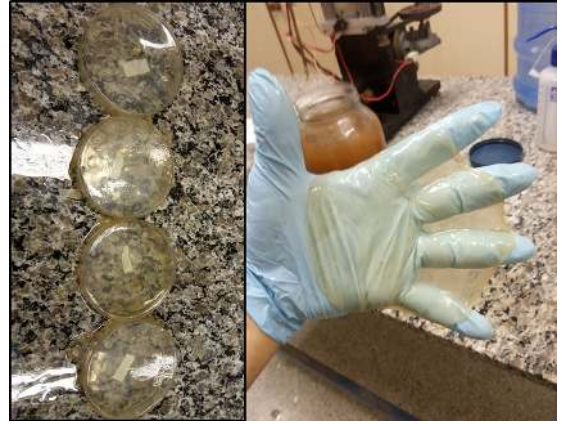


Figure 1. Characteristic of the films developed by the four different concentrations of *Maytenus rigida* Mart.

adhesion. Topographic homogeneity was evaluated to investigate the discontinuity of height distribution. According to Matos et al.⁴, this parameter can be calculated using the Shannon's entropy. Thus, to obtain this parameter, an algorithm similar to that of Matos et al.⁴ was developed. This procedure was necessary because no commercial software provides these measures. AFM images were converted to binary data using WSXM software. These binary data provided binary matrices of 512 x 512 pixels. Sequentially, Shannon's entropy was used to calculate the surface entropy according to Equation 3⁴¹.

$$H^{(2)} = -\sum_{i=1}^N \sum_{j=1}^N P_{ij} \cdot \log p_{ij} \quad (3)$$

where p_{ij} represents the probability that each matrix element is not inserted in the set of outliers of the height distribution. In addition, the entropy value was normalized to find uniform and non-uniform height distribution patterns using Equation 4⁴.

$$H_{matr\ alt} = \frac{H^{(2)} - H_{min}^{(2)}}{H_{max}^{(2)} - H_{min}^{(2)}} \quad (4)$$

where $H_{max}^{(2)}$ represents the surface with minimum uniform patterns and $H_{min}^{(2)}$ represents the non-uniform pattern surface. A box plot defined that the uniform patterns had a value of 1 while the non-uniform patterns 0. We focused in $H_{max}^{(2)}$ values that were represented by the H symbol. The model was developed in R language using the free software Rstudio version 1.2.5033.

2.6. Fractal parameters

The fractal dimension (FD) is a parameter that can be associated with surface texture⁴². However, this parameter does not quantify the texture homogeneity because different textures can have the same fractal dimension. Thus, FD has been combined with fractal lacunarity (FL)⁴³. FL is associated with the distribution of gaps on the surface. Another essential superficial parameter, fractal succolarity (FS), too should be considered for a complete description

of the fractal behavior of samples. This parameter measures the percolation of a surface²⁴.

The FD was computed using the box counting method by MountainsMap Premium software version 8.4.8872, The other two parameters are not provided by any commercial software, and therefore two different algorithms were developed in R (for FS) and Fortran (for FL), respectively. These algorithms were based on the models previously described by Talu et al.⁴⁴. After a few initial steps, SF was calculated according to Equation 5⁴⁵.

$$FS(T(k), dir) = \frac{\sum_{k=1}^n P_0(T(k)) \cdot PR(T(k), p_c)}{\sum_{k=1}^n PR(T(k), p_c)} \quad (5)$$

where *dir* is the water inlet direction, T(k) is boxes of equal sizes T(n), P₀(T(k)) is the occupation percentage, PR is the occupation pressure, and p_c is the centroid's position (x, y) of pressure applied to the calculated box.

Likewise, FL can be calculated using Equation 6 through the differential box counting method²⁴ as described by Talu et al.⁴⁴.

$$L(r) = \frac{M2}{[M1]^2} \quad (6)$$

where FL(*r*) is the lacunarity and $M1 = \sum s.P(s, r)$ and $M2 = \sum s^2.P(s, r)$ are the first and second moments of the frequency distribution of the mass of the box in differential box counting method, respectively. Finally, the power law described by Equation 7⁴⁶ was applied.

$$FL(r) = \alpha \cdot r^\beta \quad (7)$$

where α is an arbitrary constant and *r* is the box size in differential box counting method. The lacunarity coefficient β was estimated as the angular coefficient of the $\log(r)$ versus $\log[1+FL(r)]$ curve. The curve shift was necessary because the lacunarity values were very small.

2.7. Contact angle

The contact angle was obtained by sessile drop method. A homebasic system developed to take the images. A digital camera (Haiz, China) operating with a focus range of 0 ~ 200 mm was employed. All datas were taken with humidity of $51 \pm 5\%$ and temperature of $26 \pm 2^\circ\text{C}$. Image J software (Java version 1.6.005) was used to images process. Three measurements were taken of each sample in different regions for obtain experiment precision.

2.8. Statistical analysis

Statistical analyses were taken using OriginPro[®] software trial version 8.5. Variance analysis (ANOVA) was used with a tukey-test at a p-value of 0.05. To obtain the experiment precision in AFM analysis were taken four measures, while in the contact angle three measures were performed.

3. Results and Discussion

3.1. Evaluation of the chemical interaction of the biofilms compounds

The FTIR spectra of the *Maytenus rigida* powder and films are shown in Figure 2. The incorporation of *Maytenus rigida* extract in the substrates of the films promoted chemical interaction between the compounds of the extract and the EPS matrix. According to Estevam et al.¹⁶ the hydroethanolic extract of *Maytenus rigida* is designed to have several compounds, mainly, Phenols, Flavonoids, Quinones, Tannins and Triterpenes. The spectrum related to the *Maytenus rigida* powder in our extract revealed a molecular structure equivalent to hydrolyzable tannins. This structure was similar to that found by Lima et al.⁴⁷, where a strong band at $\sim 3410\text{ cm}^{-1}$ related to O-H vibration was observed. The main vibrations related to the aromatic tannin rings (related to C=C) present in the extract were registered between ~ 1325 and 1680 cm^{-1} . Moreover, a band was also computed around 835 cm^{-1} that we attributed to CO_2 vibration. The spectrum related to pure EPS matrix (Bio0) also has a band related to hydroxyl groups at 3280 cm^{-1} , as well as symmetric and antisymmetric stretching vibration of C-H related to CH_3 and CH_2 between ~ 2830 and 2870 cm^{-1} . Futher, between ~ 1480 and 1700 cm^{-1} , a band associated with the bending mode of O-H in molecular water was computed. Finally, from ~ 900 - 1180 cm^{-1} an intense band related to the stretching vibration of carbohydrate rings was observed, which comprises a fingerprint region of Dextran, as previously reported by Coma et al.².

The addition of *Maytenus* extract in the films showed a band between 3700 - 3100 cm^{-1} , mainly in Bio25 and Bio50, referring to the O-H vibration of carbohydrates and hydroxyl groups related to molecular water present in the EPS matrix. There is a great reduction in this group for the higher *Maytenus* content, which suggests that the EPS matrix has become more hydrophobic. Also characteristic bands of C-H vibration associated with alkane groups were observed between the region of 3000 - 2800 cm^{-1} . At 1640 cm^{-1} , an intense band referring to C = C of the aromatic rings of *Maytenus* was recorded. Between 1500 and 1300 cm^{-1} , bands referring to C-H vibrations of aromatic rings and COO- of carboxylic groups are observed. At 1325 cm^{-1} , vibrations related to C = C of aromatic rings were observed, while between 1200 - 950 cm^{-1} , characteristic vibrations of carbohydrates

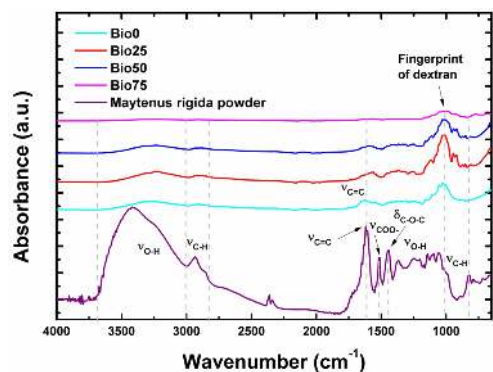


Figure 2. FTIR spectra of *Maytenus rigida* powder and EPS-based films.

were recorded. At 896 cm^{-1} , the presence of C-H bands characteristic of cellulose groups was noted, as a result of the loading of Maytenus compounds onto the EPS matrix. The chemical interaction between Tannins and the EPS matrix was due to the fact that tannin compounds can easily bind with other organic molecules⁴⁸, which promoted the great interaction between the EPS matrix and the compounds when the Maytenus content increased. Explicitly, most bands decrease significantly in Bio75, probably because the EPS matrix chelated the extract in its structure.

3.2. Wetability analysis

The drops deposited on the films developed with the different concentrations of the plant extract are displayed in Figure 3. In addition, the measurements of the angles obtained by processing the images revealed that all films had hydrophilic feature. Although ANOVA has detected a significant difference between the films, Bio0 ($57.87 \pm 4.45^\circ$), Bio25 ($54 \pm 4.31^\circ$) and Bio50 ($58.27 \pm 3.07^\circ$) exhibited similar contact angles, while Bio75 ($88.8 \pm 5.83^\circ$) had the largest contact angle, confirming that the extract compounds interact chemically with the EPS matrix making it more hydrophobic. For applications in regenerative medicine it is ideal that the films have low contact angles to be more hydrophilic and interact quickly with the skin²³. Our results were also very similar to other works reported on kefir biopolymer, which is a polysaccharide synthesized by the lactic acid bacteria of kefir grains^{49,50}. Furthermore, our films were more hydrophilic than chitosan biofilms^{51,52}.

3.3. Morphology analysis

2D and 3D views of single representative images selected, one per each sample with and without *Maytenus rigida* extract incorporated are displayed in Figure 4. These images revealed the films microstructure in a color scale. The biofilm without extract Bio0 showed rough trails along the image due to bacteria that are randomly distributed along the surface. Likewise, when the extract was added (Bio25 to Bio75), the material's microstructure underwent changes according to the increase in the extract concentration. Structures similar to yeasts were better visualized at higher concentrations of the extract (Figure 4c), while bacteria were seen in at lower concentration (Figure 4b).

The study of surface morphology has become essential for the characterization of biological systems. In this regard, AFM can provide accurate images, revealing important details of these types of systems, e.g.,^{53,54}. Although our measurements have been obtained in the air the characteristics and shapes of the biofilm did not changed, on drying in air. As noted, the images showed that the surface of the biofilms was greatly affected by the incorporation of *Maytenus rigida* extract. This behavior may be related to the chemical nature of plant compounds. According to de Araújo et al.⁵⁵ and Fernández-Bobey et al.⁵⁶, *Maytenus rigida* is a plant rich in Terpenoids and Tannins. Most of these compounds can provide alcoholic extracts, which added the largest fermentation to the biofilm formation process.

In fact, from Bio25 to Bio75, the structural changes may be due to an increase in the fermentation process that promoted a chemical interaction between the compounds of the polymer matrix and extract compounds. As the microbiota composition of kefir grains is formed by bacteria and yeasts^{57,58}, high fermentation can activate more predominant yeasts. Figure 4d reveals the contours associated with the bacteria (yellow region) that are deposited along the exopolysaccharide matrix. At this concentration, fermentation promotes the predominance of bacteria more than yeast, which was also observed by Ferraro et al.¹³ for kefir biofilms prepared with *Theobroma grandiflorum* Shum juice. However, as it was possible to observe in Figures 4c and 4d, the structures had larger contours that we associate with yeasts (more yellow region). These observations were also discussed by Almeida et al.¹² for kefir biofilms associated with *Euterpe oleracea* Mart. From Bio50 to Bio75 there was still a transition in the structure morphology, because Bio75 biofilm had character more rough.

The results of the surface parameters exhibited no significant differences ($p > 0.05$), showing that although a variation in the average value was observed, biofilms exhibited similar height spatial distribution (Table 1). Our biofilms exhibited less roughness than those observed by Matos et al.⁴. If biofilms are designed as biocuratives, for example, very rough surfaces can "stick" the cells when they interact with the biofilm surface. Furthermore, Bio25 biofilm had more hydrophilic surface, as observed

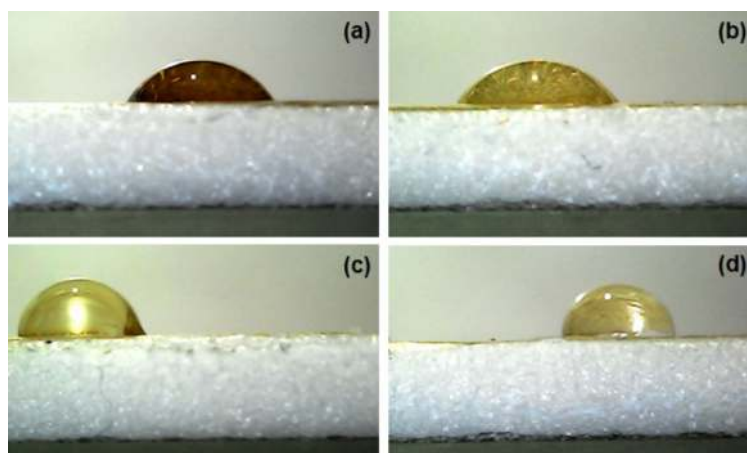


Figure 3. Contact angle of kefir biofilms loaded with *Maytenus rigida* extract: a) Bio0, b) Bio25, c) Bio50, and d) Bio75.

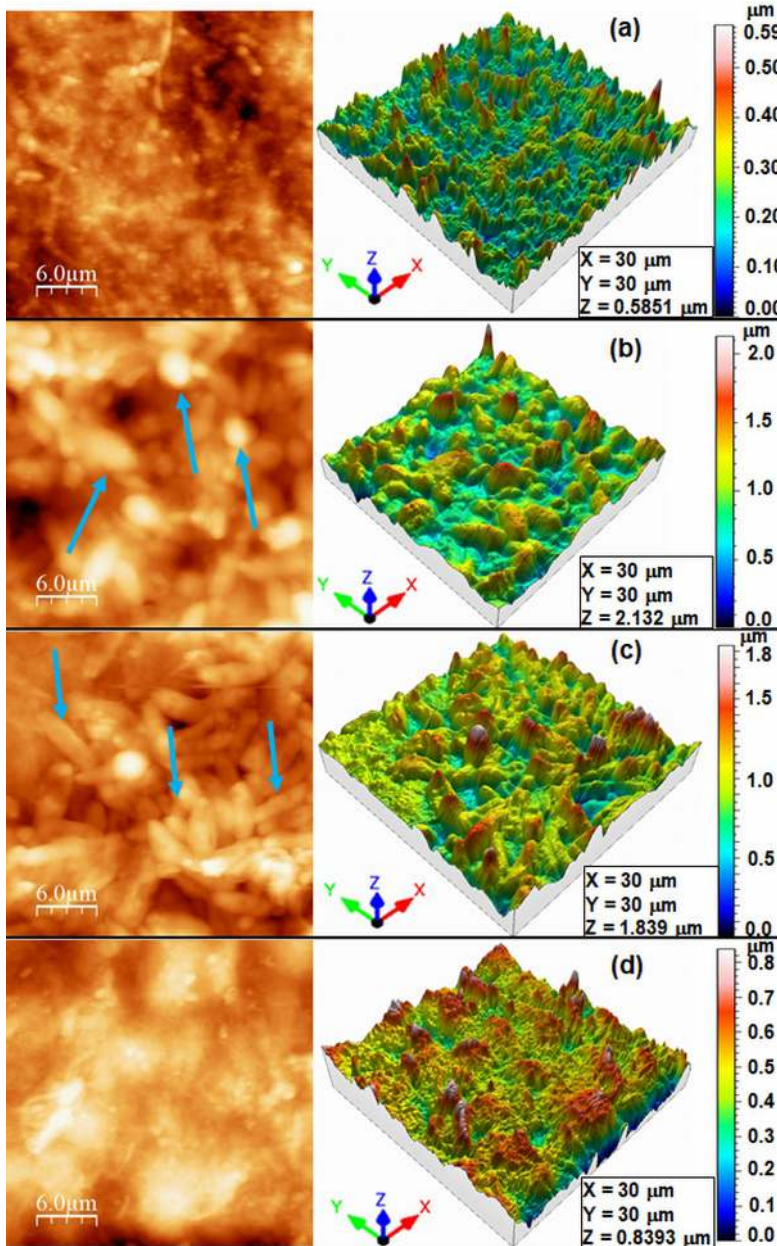


Figure 4. Relevant 2D and 3D AFM micrographs of samples: a) Bio0, b) Bio25, c) Bio50, and d) Bio75. Blue arrows indicate bacteria in b) and yeasts in c).

Table 1. More relevant superficial parameters S_q and R_{sk} . The average results were expressed as mean value and standard deviation.

Parameter	Units	Bio0	Bio25	Bio50	Bio75
S_q	nm	162.6 ± 60.6	222.9 ± 169.0	335.3 ± 94.4	575.5 ± 388.6
R_{sk}	-	0.13 ± 0.4	-0.03 ± 0.4	0.30 ± 0.2	-0.06 ± 0.5

in section 3.1, suggesting that this concentration seems to produce the film with better surface characteristics for application in regenerative medicine. The surface asymmetry, which is a parameter that quantifies whether the asymmetry is positive or negative^{44,59}, presented no significant difference ($p > 0.05$). However, it was observed that the asymmetry values were close to zero. This fact is important because films of biomedical interest must be designed to interact

evenly with biological surfaces. As a biocurative, it would be expensive to have a dressing removed due to problems of heterogeneity in adherence.

3.4. Surface microtexture

Through image processing using MountainsMab the furrows and contours lines generated by the rough peaks on the biofilm surface were obtained. Figure 5. show the furrows

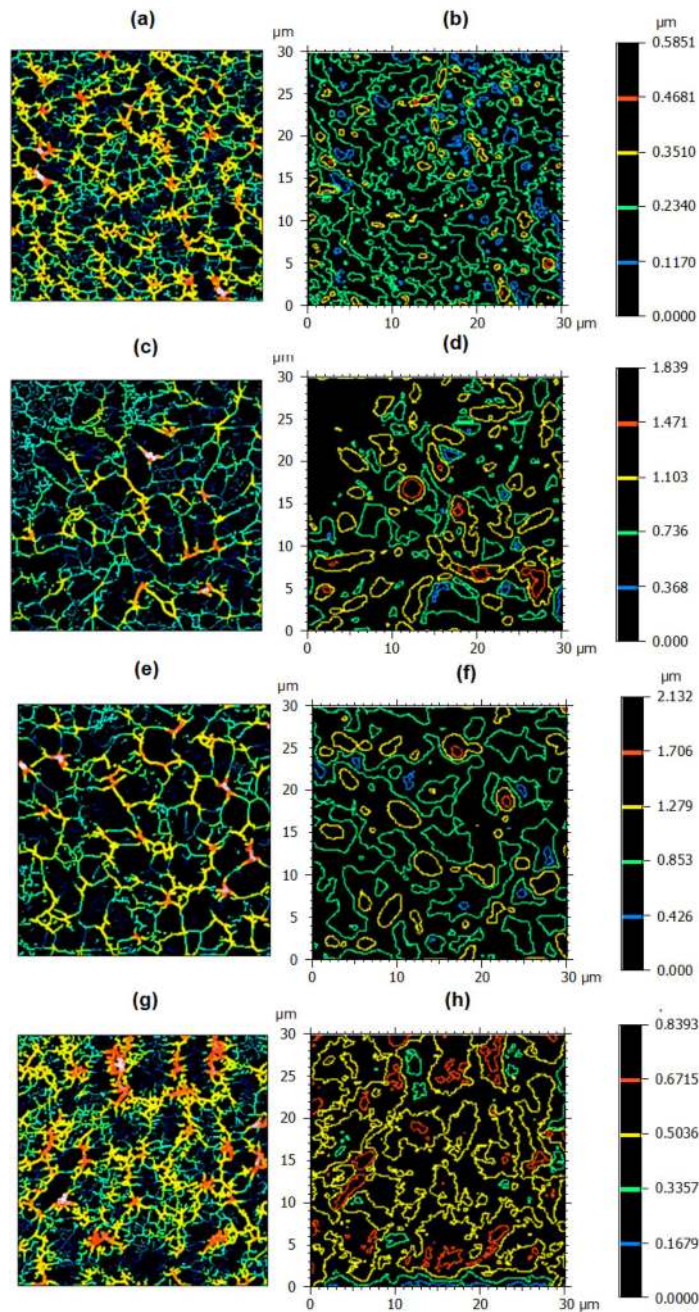


Figure 5. Graphical representations of the furrows and lines contours for a,b) Bio0, c,d) Bio25, e,f) Bio50, and g,h) Bio75.

and contour lines for each biofilm, respectively. It was observed that the addition of the plant extract promoted changes in the presentation of the furrows and contours. The furrows and contours for the biofilm without the extract (Figures 5a and 5b) were smooth, with the distribution of micro-furrows showing dispersed throughout the exopolysaccharide matrix. The contour lines (Figures 5b, 5d, 5f, and 5h) also revealed how the surfaces can behave when they are flooded by some fluid. Some macro-regions would be more exposed to higher concentrations of the plant extract.

The microtexture of a material is strongly affected by roughness and others surface parameters³⁷. In short, larger

structures were observed for biofilms with plant extract than those without, as shown in Figure 4. Again, this is due to the chemical biofilm formation process. The triterpene compounds in the extract interact with the sugars to develop the growth of these structures on the surface. It is also worth noting that the lowest concentration of the extract (Figure 5c, d) offered the best wettability, given the larger area flooded. There were more valleys than peaks filled with pseudo-fluid for this sample than for any other.

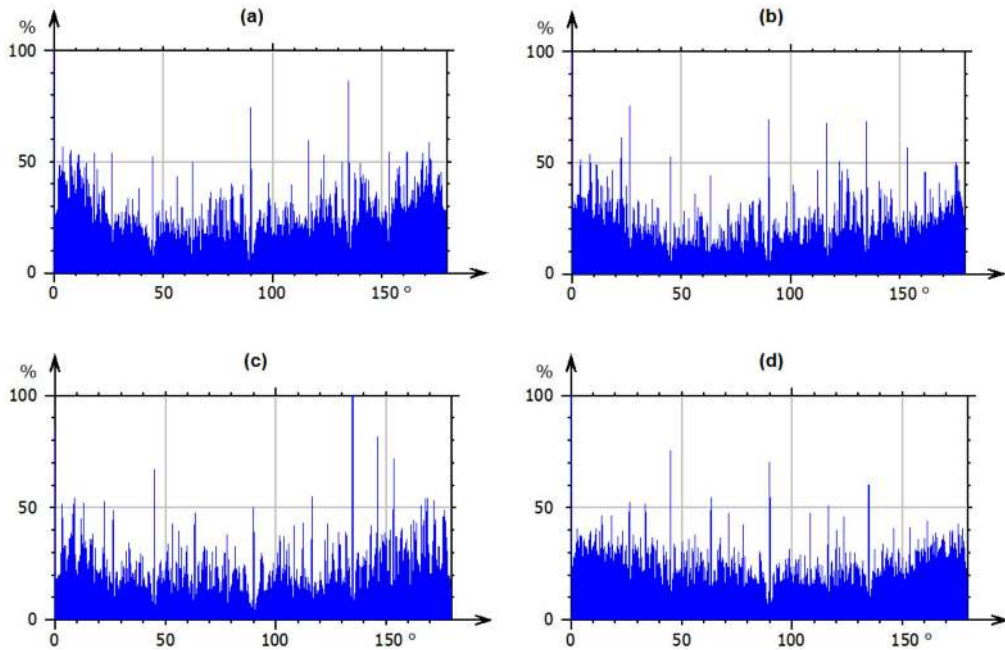
Table 2 shows the values associated with furrows. The maximum depth of the furrows was greater for Bio25 and less for Bio0. In addition, from Bio25 to Bio75, the maximum

Table 2. The parameters of furrows of the samples.

Parameter	Units	Bio0	Bio25	Bio50	Bio75
Maximum depth of furrows	μm	0.301	1.172	1.109	0.3794
Mean depth of furrows	μm	0.1243	0.3830	0.4547	0.1638
Mean density of furrows	cm/cm^2	11082	8964	7269	11317

Table 3. Surface Texture Isotropy (STI) and their respective directions for more relevant analyzed samples.

Parameter	Units	Bio0	Bio25	Bio50	Bio75
STI	%	74.78	87.79	73.75	62.02
First Direction	$^\circ$	180	0.0252	135	180
Second Direction	$^\circ$	135	26.45	0.001649	0.001649
Third Direction	$^\circ$	90	90	146.2	90

**Figure 6.** The representation of surface texture directions of the more relevant analyzed samples for a) Bio0, b) Bio25, c) Bio50, and d) Bio75.

depth decreases. However, the average depth was higher for Bio50 and lower for Bio0. The average density of furrows per area was higher for Bio75 and lower for Bio50. From Bio25 to Bio50, it decreased and grew back to Bio75. Although samples Bio25 and Bio50 had the average depth of the different furrows, these samples were the largest and closest to each other. In this sense, they would be the ones that could most absorb the pseudo-fluid in the channels generated by the difference between valleys and peaks. These results are also in accordance with wettability datas. Samples with smaller mean depths can be permeated completely more quickly than samples with greater differences between peaks and valleys.

Figure 6 shows the texture distribution for each studied biofilm. Quantitative data are presented in Table 3. The greatest dispersion in relation to the texture direction occurred for biofilm Bio0. This biofilm presented three directions with specific angles, as well as the biofilm with extract Bio75. The difference, however, was in the second texture direction (135° versus 45°). Samples Bio25 and Bio50 also differ in first and second directions, respectively.

The texture distribution is an essential parameter to understand the microtexture behavior of a material³⁸. The results presented in Figure 6 combined with the data in Table 3 revealed that the highest texture isotropy was computed for biofilm Bio25 (87.79%). For these results, this sample is more isotropic than the others, in other words, their physical properties vary less with the texture direction^{60,61}. In contrast, the most anisotropic sample was Bio75 (62.02%), probably because the growth of yeasts was disordered and random. When the surface has very different sized particles, it tends to be more anisotropic. Thus, sample Bio25 has an apparently more homogeneous texture distribution. However, we are interested in more quantitative analysis. Therefore, we introduced fractal parameters to fully understand about biofilms morphology and microtexture.

3.5. Fractals parameter analysis

The results presented above were very qualitative. We searched for more quantitative data to describe the behavior of surface microtexture. For this reason, we use the fractal dimension associated with three new fractal parameters such as surface entropy, fractal succolarity and

Table 4. Results of Fractal Dimension FD, Topographic Entropy (H), Fractal Succolarity (FS), and Lacunarity Coefficient (β). The average results were expressed as mean value and standard deviation.

Parameter	Bio0	Bio25	Bio50	Bio75
FD	2.1546±0.03	2.1198±0.047	2.1128±0.036	2.1032±0.036
H	0.98±0.017	0.983±0.017	0.986±0.012	0.987±0.015
FS	0.506±0.067	0.497±0.106	0.503±0.075	0.685±0.171
$ \beta $	7.57E ⁻⁶ ±4.03E ⁻⁶	6.89E ⁻⁷ ±4.63E ⁻⁸	8.19E ⁻⁶ ±1.32E ⁻⁷	2.79E ⁻⁶ ±4.50E ⁻⁶

fractal lacunarity. This was studied because fractal theory has been used extensively for the characterization of film microtexture, e.g.,^{26,60,62}. Table 4 shows the values associated with these four parameters analyzed. The fractal dimension showed no significant difference ($p>0.05$) between the biofilms, showing that spatial complexity was similar. According to Mandelbrot and Wheeler⁴², objects with the same fractal dimension can have different textures. For this reason, we seek other fractal parameters to differentiate the surface microtexture.

Likewise, surface entropy showed values very close to 1, without significant difference ($p>0.005$). This showed that the height distribution was strongly uniform for all biofilms. In a recent study, Matos et al.⁴ showed that kefir biofilms associated with the extract of *Euterpe oleracea* Mart. and *Theobroma grandiflorum* Shum also had $H \sim 1$. In addition, Țălu et al.^{29,44} showed that this model applies perfectly to film uniformity. The surface entropy can be related to the uniformity of superficial adhesion⁴. As there was a high topographic entropy, the possibility of the surface adhesion being uniform throughout the biofilms is also high because there is less possibility of discontinuous points being observed along the surface. Furthermore, fractal succolarity has identified no significant differences ($p>0.05$) between biofilms. This was in contrast to the results obtained for the wettability of the films, since succolarity is related to surface percolation. However, the values were close to 0.5, which according to Melo and Conci⁴⁵ and de Oliveira et al.⁶³ it is an ideal surface percolation value.

On the other hand, the lacunarity coefficient β presented significant difference ($p<0.05$) and the lowest value was observed for Bio25. In fact, according to Salcedo et al.²⁴, this directly affects the surface microtexture. When the value of $|\beta|$ is lower, the surface is less lacunar and has a more homogeneous microtexture, because there is a greater similarity between the gaps sizes distributed on the surface⁶¹. Thus, Bio25 had a more homogeneous microtexture.

Therefore, when comparing the results obtained for the material's morphology and microtexture aspects, we understand that there is a synergistic relationship. The biofilm with the lowest concentration of extract presented the appropriate microorganisms to develop on the surface and the most homogeneous microtexture. A possible application for this material would be as a natural dressing. In fact, these microorganisms could act against other pathogens. Its optimized morphology associated with the antimicrobial properties of the *Maytenus rigida* extract could attribute an excellent functional activity to this material.

4. Conclusions

In this research, we studied the morphology and microtexture of kefir biofilms associated with the *Maytenus rigida* extract. Biofilms were synthesized using substrates with different concentrations of the plant extract. The incorporation of the extract promoted chemical interaction between the compounds, which culminated in the decrease of characteristic bands of compounds of the extract, as a result of the chelating effect of the EPS matrix. The films Bio25 and Bio50, as well as Bio0 exhibited lower contact angles, revealing high surface wettability. AFM images revealed that the morphology was more smooth for the biofilm with lower extract. Structures associated with bacteria present in the kefir grains microbiota were prevailing in Bio25. Surface roughness and surface asymmetry presented suitable values for Bio25. The microtexture exposed isotropic behavior for Bio25, while Bio75 was more anisotropic. The fractal parameters showed that the most homogeneous microtexture also occurred for Bio25. All of these results were linked with the biofilm formation process. Thus, our results suggest that Bio25 presents suitable morphological parameters for biomedical application. Furthermore, in general the higher low cost of demerara sugar makes these biofilms a more viable alternative than other biofilms grown in brown sugar previously reported. However, other studies still need to be carried out, such as mechanical properties, *in vitro*, and *in vivo* tests, to assign consistent application to these biofilms. Nevertheless, the physics tools applied in the surface characterization of biofilms were sufficient to show how the plant extract affected the physics parameters of this polymeric microbial film.

5. Acknowledgments

The authors thank Coordenação de Aperfeiçoamento de Pessoal de Nível Superior (CAPES) for the financial support, as well as the use of the infrastructure of the Analytical Center of Universidade Federal do Amazonas (UFAM).

6. References

1. Piermaria JA, Pinotti A, Garcia MA, Abraham AG. Films based on kefir, an exopolysaccharide obtained from kefir grain: development and characterization. *Food Hydrocoll.* 2009;23(3):684-90.
2. Coma ME, Peltzer MA, Delgado JF, Salvay AG. Water kefir grains as an innovative source of materials: study of plasticiser content on film properties. *Eur Polym J.* 2019;120(July):109234.
3. Pop CR, Salanță L, Rotar AM, Semeniuc CA, Socaci C, Sincic M. Influence of extraction conditions on characteristics of microbial polysaccharide kefirin isolated from kefir grains biomass. *J Food Nutr Res.* 2016;55(2):121-30.

4. Matos RS, Lopes GAC, Ferreira NS, Pinto EP, Carvalho JCT, Figueiredo SS, et al. Superficial characterization of Kefir biofilms associated with açai and cupuaçu extracts. *Arab J Sci Eng.* 2018;43(7):3371-9.
5. Ghasemlou M, Khodaiyan F, Oromiehie A. Rheological and structural characterisation of film-forming solutions and biodegradable edible film made from kefir as affected by various plasticizer types. *Int J Biol Macromol.* 2011;49(4):814-21.
6. Pop C, Apostu S, Rotar AM, Semeniuc CA, Sindic M, Mabon N. FTIR spectroscopic characterization of a new biofilm obtained from kefir. *J Agroalim Process Technol.* 2013;19(2):157-9.
7. Sun G, Mao JJ. Engineering dextran-based scaffolds for drug delivery and tissue repair. *Nanomedicine (Lond).* 2012;7(11):1771-84.
8. Draye J-P, Delaey B, Van de Voorde A, Van Den Bulcke A, De Reu B, Schacht E. In vitro and in vivo biocompatibility of dextran dialdehyde cross-linked gelatin hydrogel films. *Biomaterials.* 1998;19(18):1677-87.
9. Brunsen A, Ritz U, Mateescu A, Höfer I, Frank P, Menges B, et al. Photocrosslinkable dextran hydrogel films as substrates for osteoblast and endothelial cell growth. *J Mater Chem.* 2012;22(37):19590.
10. Zheng C, Liu C, Chen H, Wang N, Liu X, Sun G, et al. Effective wound dressing based on Poly (vinyl alcohol)/Dextran-aldehyde composite hydrogel. *Int J Biol Macromol.* 2019;132:1098-105.
11. Tchobanian A, Ceyssens F, Córdor Salgado M, Van Oosterwyck H, Fardim P. Patterned dextran ester films as a tailorable cell culture platform. *Carbohydr Polym.* 2021;252:117183.
12. Almeida PA, Pinto EP, Fonseca HD Fo, Matos RS. Distribution of microorganisms on surface of Kefir biofilms associated with Açai extract Distribution of microorganisms on surface of Kefir biofilms associated with Açai extract. *Sci Amaz.* [serial on the Internet]. 2019;8(3):C10-8. [cited 2021 Dec 29]. Available from: <http://www.scientia-amazonia.org>
13. Ferraro MAN, Pinto EP, Matos RS. Study of the superficial distribution of microorganisms in kefir biofilms prepared with Cupuaçu juice. *J Bioenergy Food Sci.* 2020;7:1-11.
14. Carriconde C. Bom nome, *Maytenus rigida*, Mart. *De Volta às Raízes.* 2004;19:1-2.
15. Santos VL, Souza MFV, Batista LM, Silva BA, Lima MS, Souza AMF, et al. Avaliação da atividade antimicrobiana de *Maytenus rigida* Mart. (Celastraceae). *Rev Bras Plantas Med.* 2011;13(1):68-72.
16. Estevam CS, Cavalcanti AM, Cambui ÉVF, Araújo V No, Leopoldo PTG, Fernandes RPM, et al. Perfil fitoquímico e ensaio microbiológico dos extratos da entrecasca de *Maytenus rigida* Mart. (Celastraceae). *Rev Bras Farmacogn.* 2009;19(1b):299-303.
17. Oliveira JFS, Bastos MLA, Verissimo RCSS, Araújo-Júnior JX, Bernardo THL. Phytochemical profile and evaluation of antibacterial and cytotoxic activity of *Maytenus rigida* (Mart.) extracts and fractions. *J Chem Pharm Res.* 2016;8(July):746-51.
18. Zolfi M, Khodaiyan F, Mousavi M, Hashemi M. Development and characterization of the kefir-whey protein isolate-TiO₂ nanocomposite films. *Int J Biol Macromol.* 2014;65:340-5.
19. Babaei-Ghazvini A, Shahabi-Ghahfarrokhi I, Goudarzi V. Preparation of UV-protective starch/kefir/ZnO nanocomposite as a packaging film: characterization. *Food Packag Shelf Life.* 2017;2018(16):103-11. <http://dx.doi.org/10.1016/j.ftp.2018.01.008>.
20. Barcelay YR, Moreira JAG, de Jesus Monteiro Almeida A, Brito WR, Matos RS, da Fonseca HD Fo. Nanoscale stereometric evaluation of BiZn_{0.5}Ti_{0.5}O₃ thin films grown by RF magnetron sputtering. *Mater Lett.* 2020;279:128477.
21. Wright CJ, Shah MK, Powell LC, Armstrong I. Application of AFM from microbial cell to biofilm. *Scanning.* 2010;32(3):134-49.
22. Ramos GQ, Matos RS, da Fonseca HD Fo. Advanced microtexture study of *Anacardium occidentale* L. Leaf surface from the Amazon by fractal theory. *Microsc Microanal.* 2020;26(5):989-96.
23. Matos RS, Ramos GQ, da Fonseca HD Fo, Țălu Ș. Advanced micromorphology study of microbial films grown on Kefir loaded with Açai extract. *Micron.* 2020;137:102912.
24. Salcedo MOC, Zamora RRM, Carvalho JCT. Study fractal leaf surface of the plant species *Copaifera* sp. using the Microscope Atomic-Force-AFM. *Rev ECIPerú.* 2016;13(1):10-6. <http://dx.doi.org/10.33017/RevECIPeru2016.0002>.
25. Dallaeva DS, Tomanek P. AFM study of structure influence on butterfly wings coloration. *Adv Electr Electron Eng.* 2012;10(2):120-4.
26. Țălu Ș, Bramowicz M, Kulesza S, Solaymani S. Topographic characterization of thin film field-effect transistors of 2,6-diphenyl anthracene (DPA) by fractal and AFM analysis. *Mater Sci Semicond Process.* 2018;79:144-52.
27. Wang B, Tang Y, Oh Y, Lamb NW, Xia S, Ding Z, et al. Controlled release of dexamethasone sodium phosphate with biodegradable nanoparticles for preventing experimental corneal neovascularization. *Nanomedicine.* 2019;17:119-23. <http://dx.doi.org/10.1016/j.nano.2019.01.001>.
28. Ito RM, de Souza CC, Gandarilla AMD, de Oliveira LM, Brito WR, Sanches EA, et al. Micromorphology and microtexture evaluation of poly(o-ethoxyaniline) films using atomic force microscopy and fractal analysis. *J Polym Res.* 2020;27(10):299.
29. Țălu Ș, Matos RS, Pinto EP, Rezaee S, Mardani M. Stereometric and fractal analysis of sputtered Ag-Cu thin films. *Surf Interfaces.* 2020;21:100650.
30. Țălu Ș, Achour A, Solaymani S, Nikpasand K, Dalouji V, Sari A, et al. Micromorphology analysis of TiO₂ thin films by atomic force microscopy images: the influence of postannealing. *Microsc Res Tech.* 2019; 83(5):457-63. <http://dx.doi.org/10.1002/jemt.23433>.
31. Sobola D, Talu S, Sadovsky P, Papez N, Grmela L. Application of AFM measurement and fractal analysis to study the surface of natural optical structures. *Adv Electr Electron Eng.* 2017;15(3):569-76.
32. Shakoury R, Rezaee S, Mwema F, Luna C, Ghosh K, Jurečka S, et al. Multifractal and optical bandgap characterization of Ta₂O₅ thin films deposited by electron gun method. *Opt Quantum Electron.* 2020;52(2):95.
33. Santos LC. Avaliação da atividade biológica da fração hexânica da entrecasca de *Maytenus rigida* Mart. [trabalho de conclusão de curso]. São Cristóvão: Universidade Federal de Sergipe; 2017 [cited 2021 Dec 29]. Available from: [https://ri.ufs.br/bitstream/riufs/6735/2/Ludmila Cruz dos Santos.pdf](https://ri.ufs.br/bitstream/riufs/6735/2/Ludmila%20Cruz%20dos%20Santos.pdf)
34. Matos RS, Pinheiro BS, Souza IS, Paes de Castro RR, Ramos GQ, Pinto EP, et al. 3D micromorphology evaluation of kefir microbial films loaded with extract of Amazon rainforest fruit Cupuaçu. *Micron.* 2021;142:102996.
35. Matos RS, Gonçalves ECM, Pinto EP, Lopes GAC, Ferreira NS, Resende CX. Nanoscale morphology, structure and fractal study of kefir microbial films grown in natura. *Polímeros.* 2020;30(3):e2020033.
36. Silva MRP, Matos RS, Estevam CS, Santos SB, da Silva FMA, Sousa IGPP, et al. Structural evaluation of polymeric microbial films grown on kefir loaded with *Maytenus rigida* extract. *Microsc Res Tech.* 2021;84(4):627-38.
37. Blateyron F. Characterisation of areal surface texture. USA: Springer-Verlag Berlin Heidelberg; 2013. <http://dx.doi.org/10.1007/978-3-642-36458-7>.
38. Blateyron F. The areal field parameters. In: Leach R, editor. Characterisation of areal surface texture. USA: Springer Berlin Heidelberg; 2013. p. 15-43. http://dx.doi.org/10.1007/978-3-642-36458-7_2

39. Franco LA, Sinatora A. 3D surface parameters (ISO 25178-2): actual meaning of Spk and its relationship to Vmp. *Precis Eng.* 2015;40:106-11.
40. Khulbe K, Feng C, Matsuura T. *Synthetic polymeric membranes*. USA: Springer Berlin Heidelberg; 2008. <http://dx.doi.org/10.1007/978-3-540-73994-4>.
41. Bulinski A, Dimitrov D. Statistical estimation of the shannon entropy. *Acta Math Sin Engl Ser.* 2019;35(1):17-46.
42. Mandelbrot BB, Wheeler JA. The fractal geometry of nature. *Am J Phys.* 1983;51(3):286-7.
43. Xia Y, Cai J, Perfect E, Wei W, Zhang Q, Meng Q. Fractal dimension, lacunarity and succolarity analyses on CT images of reservoir rocks for permeability prediction. *J Hydrol (Amst).* 2019;579:124198.
44. Țălu Ș, Abdolghaderi S, Pinto EP, Matos RS, Salerno M. Advanced fractal analysis of nanoscale topography of Ag/DLC composite synthesized by RF-PECVD. *Surf Eng.* 2020;36(7):713-9.
45. de Melo RHC, Conci A. Succolarity: defining a method to calculate this fractal measure. In: 2008 15th International Conference on Systems, Signals and Image Processing; 2008; Bratislava, Slovakia. Proceedings. USA: IEEE; 2008. p. 291-4. <http://dx.doi.org/10.1109/IWSSIP.2008.4604424>.
46. de Lucena LRR, Cunha M Fo. Lacunarity as index of evaluation of wind direction in Pernambuco. *Rev Bras Biometria.* 2019;37(1):95. <http://dx.doi.org/10.28951/rbb.v37i1.362>.
47. Lima RJC, Moreno AJD, Castro SFL, Gonçalves JRS, Olivera AB, Sasaki JM, et al. Taninos hidrolisáveis em Bixa orellana L. *Quim Nova.* 2006;29(3):507-9.
48. Simon C, Barathieu K, Laguerre M, Schmitter JM, Fouquet E, Pianet I, et al. Three-dimensional structure and dynamics of wine Tannin–Saliva protein complexes. A multitechnique approach †. *Biochemistry.* 2003;42(35):10385-95.
49. Shahabi-Ghahfarrokhi I, Khodaiyan F, Mousavi M, Yousefi H. Effect of γ -irradiation on the physical and mechanical properties of kefiran biopolymer film. *Int J Biol Macromol.* 2015;74:343-50.
50. Zolfi M, Khodaiyan F, Mousavi M, Hashemi M. The improvement of characteristics of biodegradable films made from kefiran-whey protein by nanoparticle incorporation. *Carbohydr Polym.* 2014;109:118-25.
51. Pinto E, Tavares W, Matos R, Ferreira A, Menezes R, Costa M, et al. Influence of low and high glycerol concentrations on wettability and flexibility of chitosan biofilms. *Quim Nova.* 2018;41(10):1109-16.
52. Silva SS, Goodfellow BJ, Benesch J, Rocha J, Mano JF, Reis RL. Morphology and miscibility of chitosan / soy protein blended membranes. *Carbohydr Polym.* 2007;70(1):25-31.
53. Jalili N, Laxminarayana K. A review of atomic force microscopy imaging systems: application to molecular metrology and biological sciences. *Mechatronics.* 2004;14(8):907-45.
54. Dufrière YF, Martínez-Martin D, Medalsy I, Alsteens D, Müller DJ. Multiparametric imaging of biological systems by force-distance curve-based AFM. *Nat Methods.* 2013;10(9):847-54.
55. de Araújo D, Fernandes A, de Andrade R, Tavares J, da Silva M. Quality control and quantitation of catechin and epicatechin from leaves of *Maytenus rigida* Mart. *MOL2NET.* 2018:1-3. <http://dx.doi.org/10.3390/mol2net-04-05552>.
56. Fernández-Bobey A, Hernández-Torriente A, García-Pérez TH, Spengler-Salabarría I. Triterpenos con actividad anti-inflamatoria aislados de la corteza de la especie endémica *Maytenus elaeodendroides*, Griseb. *Rev Cuba Quím.* 2020;32(1):61-73.
57. Cho Y-J, Kim D-H, Jeong D, Seo K-H, Jeong HS, Lee HG, et al. Characterization of yeasts isolated from kefir as a probiotic and its synergic interaction with the wine byproduct grape seed flour/extract. *LWT.* 2018;90:535-9.
58. Gut AM, Vasiljevic T, Yeager T, Donkor ON. Characterization of yeasts isolated from traditional kefir grains for potential probiotic properties. *J Funct Foods.* 2019;58:56-66.
59. Tayebi N, Polycarpou AA. Modeling the effect of skewness and kurtosis on the static friction coefficient of rough surfaces. *Tribol Int.* 2004;37(6):491-505.
60. Yadav RP, Kumar T, Baranwal V, Vandana, Kumar M, Priya PK, et al. Fractal characterization and wettability of ion treated silicon surfaces. *J Appl Phys.* 2017;121(5):055301.
61. Kilic KI, Abiyev RH. Exploiting the synergy between fractal dimension and lacunarity for improved texture recognition. *Signal Processing.* 2011;91(10):2332-44.
62. Jing C, Tang W. Ga-doped ZnO thin film surface characterization by wavelet and fractal analysis. *Appl Surf Sci.* 2016;364:843-9.
63. de Oliveira LM, Matos RS, Campelo PH, Sanches EA, da Fonseca Filho HD. Evaluation of the nanoscale surface applied to biodegradable nanoparticles containing *Allium sativum* essential oil. *Mater Lett.* 2020;275:128111.